AGU PUBLICATIONS

JGR

Journal of Geophysical Research: Oceans

RESEARCH ARTICLE

10.1002/2014JC010306

Drifter-based estimate of the 5 year dispersal of Fukushima-derived radionuclides

I. I. Rypina[1], S. R. Jayne[1], S. Yoshida[1], A. M. Macdonald[1], and K. Buesseler[2]

[1]Department of Physical Oceanography, Woods Hole Oceanographic Institution, Woods Hole, Massachusetts, USA, [2]Department of Marine Chemistry and Geochemistry, Woods Hole Oceanographic Institution, Woods Hole, Massachusetts, USA

Key Points:
- Spread of Fukushima radionuclides is studied over 5 years using drifter data
- Novel two-iteration method is employed to make the best use of drifter data
- Drifter-based results show good agreement with observations

Correspondence to:
I. I. Rypina,
irypina@whoi.edu

Citation:
Rypina, I. I., S. R. Jayne, S. Yoshida, A. M. Macdonald, and K. Buesseler (2014), Drifter-based estimate of the 5 year dispersal of Fukushima-derived radionuclides, *J. Geophys. Res. Oceans*, *119*, 8177–8193, doi:10.1002/2014JC010306.

Received 11 JUL 2014
Accepted 10 NOV 2014
Accepted article online 13 NOV 2014
Published online 28 NOV 2014

Abstract Employing some 40 years of North Pacific drifter-track observations from the Global Drifter Program database, statistics defining the horizontal spread of radionuclides from Fukushima nuclear power plant into the Pacific Ocean are investigated over a time scale of 5 years. A novel two-iteration method is employed to make the best use of the available drifter data. Drifter-based predictions of the temporal progression of the leading edge of the radionuclide distribution are compared to observed radionuclide concentrations from research surveys occupied in 2012 and 2013. Good agreement between the drifter-based predictions and the observations is found.

1. Introduction

The Fukushima nuclear power plant (FNPP) disaster in March 2011 led to a release of ^{134}Cs and other radionuclides into the Pacific Ocean [see for example, *Buesseler et al*., 2011]. The fate of these isotopes is of great importance from both scientific (tracer implications) and practical (environmental impact) viewpoints. Addressing this issue, a large number of studies published in recent literature have aimed to investigate and predict the spreading of the Fukushima-derived radionuclides in the ocean on scales from months to decades [e.g., *Kawamura et al*., 2011; *Rypina et al*., 2013; *Behrens et al*., 2012; *Dietze and Kriest*, 2012; *Estournel et al*., 2012; *Honda et al*., 2012; *Masumoto et al*., 2012; *Tsumune et al*., 2012, 2013; *Rossi et al*., 2013]. Nearly all of these predictions have been based on numerical modeling experiments. Here a different approach is taken. To study the spreading of the Fukushima-derived radionuclides over a time interval of 5 years, we make use of the large, publically available Global Drifter Program (GDP) data set representing observations of near-surface drifting buoys accumulated over several decades of field experiments. Our drifter-based estimates of spreading are compared to radionuclide concentration measurements from two recent large-scale ocean surveys to both validate our results and to interpret the radionuclide observations.

1.1. Overview of the General Circulation in the North Pacific Ocean

At basin scales, the general upper ocean horizontal circulation pattern in the North Pacific consists of the clockwise subtropical gyre and two smaller counterclockwise subpolar gyres, the Western Subarctic Gyre and the Alaskan Gyre (Figure 1). Each of these large-scale gyres contains smaller-scale features and recirculations. The subtropical and subpolar regions are separated from each other at approximately 42°N by the northern edge of the eastward flowing Kuroshio Extension (KE) Current. The KE separates warmer nutrient-poor subtropical waters from the colder nutrient-rich northern waters. KE volume transport can reach 90–140 Sv [*Wijffels et al*., 1998; *Qiu*, 2001; *Macdonald et al*., 2009; *Jayne et al*., 2009], and it is accompanied by large-amplitude meanders and energetic mesoscale eddies that strongly affect water mass formation in the region [*Tomosada*, 1986; *Talley et al*., 1995]. As the meandering KE flow transits the Pacific, it widens, and despite losing its inertial nature and dividing into multiple short-lived jets, it maintains a coherent jet-like structure past the dateline [*Qiu*, 2001; *Qiu and Chen*, 2005]. Further to the east, the KE becomes the broad North Pacific Current (a.k.a. Drift), which eventually splits to form the eastern boundary currents of subtropical and Alaskan gyres. The two subpolar systems are connected by coastal currents tracing the northern boundary along the Aleutian Island chain to the East Kamchatka and Oyashio currents in the west. The Alaskan Gyre is closed to the south at ~42°N by the North Pacific Current, while the Western Subarctic Gyre is almost triangular, squeezed close to the coast in west by the meeting of the southward flowing Oyashio

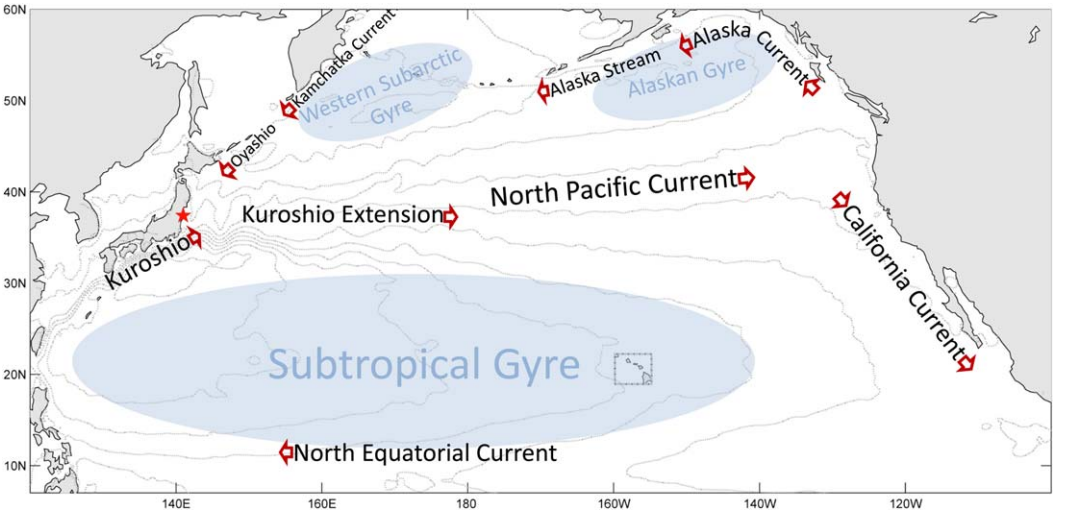

Figure 1. Rough schematic diagram of the surface currents in the North Pacific Ocean. Gray curves show select isosurfaces of the time-mean geostrophic streamfunction inferred from the AVISO sea surface heights. In this and all subsequent figures, land is shown in gray with the coastlines in black; gray/black box boundary highlights Hawaii; red star indicates FNPP location.

and the northward flowing Kuroshio entering the basin near the Boso Peninsula at about 35°N [*Talley et al*., 2011; *Reid*, 1997, and others].

At large scales, the North Pacific vertical meridional overturning circulation occurs within a bottom to deep cell and two extremely shallow, with cores at approximately 100 m, surface cells where poleward moving surface waters is balanced by equatorward subsurface flow [*Talley*, 2003; *Macdonald et al*., 2009]. In the western Pacific, just to the north of the KE, very strong surface mixing occurs seasonally, driven by winter-time storms. This deep mixing has been illustrated by winter mixed layer depths observed by Argo [e.g., *Whalen et al*., 2012, their Figures 1 and 4]. In this region, ventilated, homogeneous, low potential vorticity mode waters lie slightly above or within the permanent pycnocline. The FNPP is located on the coast just to the west of the mode water formation region. Therefore, it is not surprising that both observations and models have suggested subsurface maxima in radioisotope concentrations [*Behrens et al*., 2012; *Rossi et al*., 2013]. Nevertheless, mode water formation does not preclude the existence of detectable midbasin isotope concentrations at and near the surface [e.g., *Aoyama et al*., 2012, 2013; *Kamenik et al*., 2013; S. Yoshida et al., in preparation, 2014]. It is the spread of the surface contamination that is the focus of this study.

1.2. Brief Overview of the Spreading of Fukushima Radionuclides

Previous numerical-model-based investigations of the long-term dispersal of the Fukushima-derived radionuclides suggest that the contaminated waters would reach Hawaii by 2013 to early 2014 [*Rossi et al*., 2013], and transit across the basin to reach the U.S. west coast 3–5 years after the accident according *Rossi et al*. [2013], 4–5 years according to *Nakano and Povinec* [2012], or 5–6 years according to *Behrens et al*. [2012]. The initial radioactive tracer distribution is strongly surface intensified but penetrates to depths of more than 400 m after 3 years [*Behrens et al*., 2012; *Rossi et al*., 2013]. Both *Behrens et al*. [2012] and *Rossi et al*. [2013] suggest that by 5 years, the tracer cloud is expected to span most of the North Pacific basin, including the two subpolar gyres and the subtropical gyre, with the bulk of the tracer located off the North American coast between ~25°N and 45°N. By 10 years, this peak shrinks and shifts southward, with a secondary peak of elevated concentration appearing in the Alaskan gyre. In the far long term, after more than 30 years, about a quarter of the initial tracer amount has exited the North Pacific entering the Indian Ocean via the Indonesian Throughflow, the South Pacific after crossing the equator, and in lesser amounts the Arctic Ocean via the Bering Strait [*Rossi et al*., 2013].

1.3. Global Drifter Program Data Set

Near-surface drifting buoys or drifters are perhaps one of the oldest instruments in physical oceanography. These semi-Lagrangian instruments are ballasted to stay at the surface and have cloth sails located below the surface, which allow them to be carried by the near-surface oceanic currents. Modern drifters are equipped with a GPS-type device for locating their geographical positions, which are transmitted to shore,

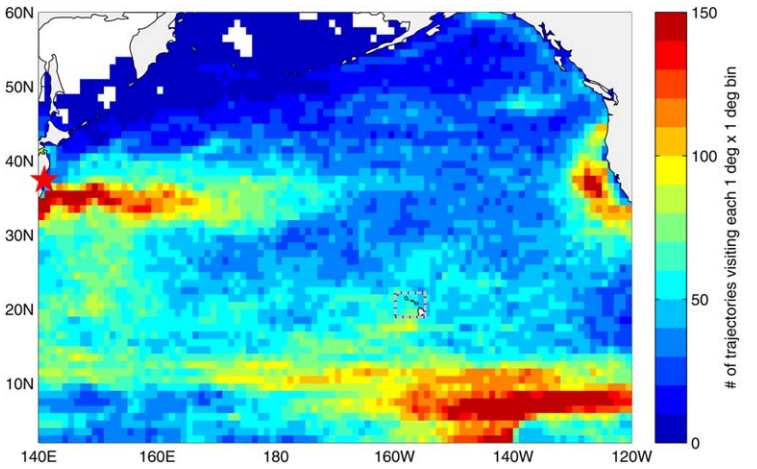

Figure 2. Data coverage map for the GDP data set. Color shows number of trajectories visiting each 1° × 1° bin throughout the North Pacific. White corresponds to areas not visited by drifters.

quality controlled and stored in the Global Drifter Program (GDP) database (http://www.aoml.noaa.gov/phod/dac/index.php). Accumulated over several decades, this global data set represents a unique resource for studying near-surface ocean circulation and processes. In the North Pacific, the basin of interest in this study, the GDP data set contains more than 6000 drifter tracks from 1979 until present, with roughly half the drifters deployed in the last 10 years. The average drifter lifetime is about 10 months, with the longest-living drifters lasting for up to 5 years. A map quantifying the number of drifters that visit each 1° × 1° spatial bin throughout the North Pacific is presented in Figure 2. Note that we counted the number of drifters visiting each box, not the total number of visits, so if trajectory visits the same bin more than once, only the first visit is counted. The data coverage is best south of 40°N, where more than 25 drifters pass, at one time or another, through each bin. The areas north of 40°N have less data but even there most bins have been visited by more than five drifters.

In this study, we use the GDP data set to investigate the spread of the Fukushima-derived radionuclides. In the next section, we introduce the notion of a probability map, which quantifies the statistics of drifter dispersal, and present the two-iteration method of computing these probability maps. Also in section 2, we present results from three numerical experiments involving simulated drifters. The two-iteration method is then applied to real drifter data in section 3, and a comparison between the drifter-based results and available observations is presented in section 4. Our results are summarized and discussed in section 5.

2. Probability Maps: Formulas, Interpretation, and Examples

From a statistical viewpoint, the expected distribution of a conservative tracer in the ocean at some time T after its release from the source area can be quantified by a probability map, showing the probability for a water parcel originating within the source area to reach different geographical locations throughout the ocean [*Rypina et al*., 2011, 2013]. Because the ocean evolves in time, the fate of a tracer depends on the timing of its release, so averaging over multiple releases is required to get a statistically stable estimate of geographical probability. For a conservative tracer, probability can be converted to tracer concentration though a renormalization by the total amount of the tracer released. For a tracer that decays with time, decay would be taken into account, in which case renormalization is based on the total tracer amount remaining in the ocean at time T after the release.

2.1. Defining Tracer Distributions From Drifter Statistics: Probability Maps

Given enough information about the 3-D trajectories of water parcels in the ocean, probability maps can be constructed to quantify the three-dimensional (lat, lon, and depth) or even the four-dimensional (lat, lon, depth, and time) distribution of a tracer. However, because GDP drifters are constrained by design to stay at or near the ocean surface, they do not provide any information about the vertical motion of water parcels. They are however, ideal as a means of investigating two-dimensional horizontal statistics. Therefore here, we ignore the vertical coordinate to create two-dimensional probability maps characterizing the probability of lateral extent in the near-surface tracer distribution. Conversion from probabilities to tracer concentrations is still possible in this case but is not as straightforward as for three-dimensional maps because it requires knowledge of the vertical structure of the tracer distribution at different geographical locations

throughout the ocean. For simplicity, we will not attempt to perform such conversion here but instead will focus on probability rather than concentration.

Given a large enough number of water parcel trajectories released from a source, for example trajectories simulated numerically using an ocean circulation model, the computation of the probability map is straightforward: thousands of trajectories are released within the source domain, the ocean is divided into small boxes of length dx and dy, and the probability that a trajectory will reach each box ij is then estimated as

$$P_{ij} = N_{ij}/N, \tag{1}$$

where N_{ij} is the number of "successful" trajectories, i.e., those that fall into the ijth box at the end of the integration time, and N is the total number of trajectories released. The probability map calculation is repeated for different trajectory integration times and, as the tracer spreads out further from the source with longer integration times, the corresponding probability maps cover ever-larger areas.

Instead of showing a sequence of probability maps at different times, it is sometimes more convenient to evolve the trajectories over the longest time of interest, and calculate the percentage of trajectories that visit each box ij at one time or another (rather than the percentage that fall into box ij at the end of the integration time),

$$P_{ij} = N_{ij}/N, \tag{2}$$

where N_{ij} is the number of successful trajectories visiting the *ij*th box at any time. Each box can be associated with the mean travel time $\overline{T_{ij}} = \frac{\sum T_{ij}}{N_{ij}}$ that is needed for a trajectory to get from the source to that box. Equation (2) is not exactly equivalent to equation (1) because different water parcels might reach the same box at different times, but the resulting probability map (P_{ij}) and the corresponding travel time map ($\overline{T_{ij}}$) together quantify where, on average, the trajectories are at any time after the release, and thus completely describe, in a statistical sense, the spreading of a tracer. Different flavors of $\overline{T_{ij}}$ are possible: time needed to initially reach the *ij*th box, time at which trajectories leave the *ij*th box, residence time within the box, etc. Here we use the first flavor defining $\overline{T_{ij}}$ as the ensemble-average time to initially reach the *ij*th box, because this choice is most convenient for comparison with observations (see section 4). So in our analysis, we focus on the first arrival of the drifters to a given geographical location (grid cell) and ignore all repeat visits of the same trajectory at later times. That is, if a trajectory visits the same bin more than once, only the first visit is counted.

2.2. Probability Map Example

To illustrate the general concept of a probability map with a more concrete example, we have constructed a realistic representation of the near-surface oceanic currents from 1992 until mid-2013 by combining AVISO gridded absolute geostrophic velocity fields (publically available from http://www.aviso.altimetry.fr/en/data.html) with Ekman currents derived from NCEP/NCAR wind stress estimates (publically available at http://www.esrl.noaa.gov/psd/data/gridded/data.ncep.reanalysis.derived.surfaceflux.html). The gridded geostrophic velocity estimates distributed by AVISO are derived from satellite-based sea surface height measurements, have near-global coverage, are available on a 1/3° Mercator grid, and have a nominal temporal resolution of 7 days. To obtain estimates of Ekman currents, we converted daily NCEP reanalysis 10 m wind stress estimates, τ, to zonal and meridional ocean velocities, u_{Ek} and v_{Ek}, using the *Ralph and Niiler* [1999] formula: $u_{Ek} + iv_{Ek} = \beta\, e^{-i\theta}/(f\rho)\,(\tau_x + i\tau_y)/\sqrt{|\tau|}$, where $\rho = 1027$ kg·m^{-3} is the assumed seawater density, f is the Coriolis parameter, $\theta = 55°$ is the rotation angle of the Ekman current, and $\beta = 0.065$ s$^{-1/2}$. For a more detailed description of the velocity field construction, see *Rypina et al*. [2013].

This velocity field is used to estimate the spread of simulated drifter trajectories from the 2° longitude by 3° latitude source domain near Fukushima into the broader Pacific Ocean over a time scale of 5 years. In this calculation, we use satellite-based velocities (described in the paragraph above) from the time period 1992 to 2013 to do monthly drifter release experiments from October 1992 through September 2007 (180 release experiments in total) and integrate trajectories forward in time over 5 years starting from the trajectory release time. In each release experiment, we seed 25 simulated drifters (five rows with five drifters in each row) on a regular rectangular grid (with spacing of 0.4° longitude and 0.6° latitude between the neighboring drifters) inside the source domain, totaling 4500 drifters for the 180 monthly releases. The 5 year

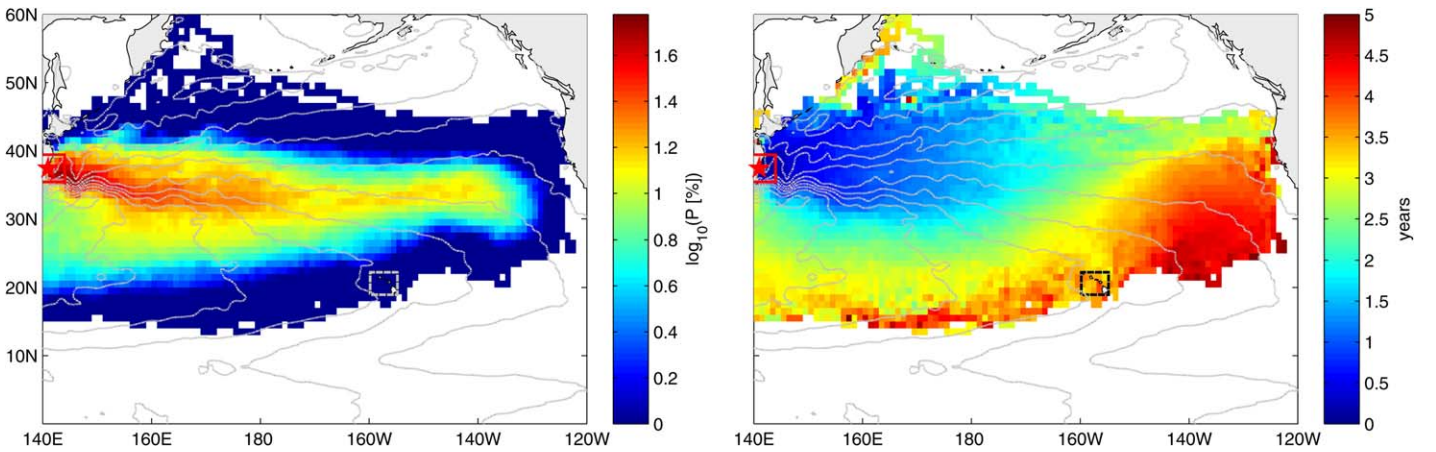

Figure 3. (left) Probability map and (right) the corresponding travel time map describing the dispersal of simulated water parcels out of the Fukushima (red star) source domain (red rectangle) into the Pacific Ocean. Simulated trajectories are advected using a combination of altimetric AVISO-based geostrophic currents and NCEP-based Ekman velocities. In this calculation, 25 simulated drifters were released in the source area (red box) once a month from October 1992 through September 2007 and trajectories were evolved for 5 years. Gray curves show select isosurfaces of time-mean geostrophic streamfunction.

construct is intended to represent both the time scale of interest for the spread of Fukushima radionuclides and the longest lifespan for a drifter. Trajectories of simulated drifters were computed using a variable-step fourth-order Runge-Kutta integration scheme with bilinear velocity interpolation in time and space between grid points.

Throughout this manuscript, we used $1^\circ \times 1^\circ$ bins to construct the probability maps. This bin size was chosen as a compromise between resolution (which favors smaller bin sizes) and precision (which favors larger bin sizes that allow more trajectories to visit each bin). As shown in Figure 2, for this bin size, more than 25 trajectories pass through most bins in the North Pacific leading to reasonable drifter statistics throughout most of the northern basin. Note also that sensitivity tests presented in Appendix A suggest that doubling the bin size in both latitude and longitude does not lead to any qualitative changes in the resulting probability map.

The choice of the source domain size is somewhat arbitrary. Smaller source domains better resemble the direct discharge from the power plant but they contain fewer trajectories from drifters that were either released in or passed through the source domain. Larger source domains, on the other hand, contain more real drifter trajectories and thus lead to better statistics, but they do not correspond so well to the physical domain where the direct ocean leakage occurred. One reason for using a larger rather than smaller source domain is that, in addition to the direct discharge, radionuclides also went into the atmosphere during FNPP explosions and were then deposited back onto the ocean surface with rain. The most concentrated atmospheric deposition of ^{137}Cs occurred soon after the explosion and relatively close to the Fukushima location. According to *Stohl et al*. [2012], about 40% of the total atmospheric deposition occurred by early April 2011 within 300 km ($\sim 3^\circ$ of latitude/longitude) of Fukushima, where surface concentrations of atmospherically deposited ^{137}Cs reached 10^5 Bq m^{-2}. The remaining 60% of the atmospheric deposition occurred over vast areas of the Pacific Ocean at much smaller concentrations that quickly diluted to low levels. The roughly 200 km $\times$ 300 km source domain box used in this study is a reasonable representation of the combined effect of the two sources of contamination, the point-source-like direct discharge and the relatively wider spread atmospheric deposition. Note also that sensitivity tests (see Appendix A) suggest that the character and statistics of resulting maps are not particularly sensitive to variations in the domain size within reasonable limits (from 1.5° to 4° or, equivalently, from about 150 to 400 km).

As might be expected from what is known about the general near-surface circulation in the Pacific Ocean, the probability and travel time maps resulting from the simulated drifter releases (Figure 3) show an eastward spread of trajectories from the source (blue to green to red in the right figure) with time. The probabilities are plotted using a logarithmic (i.e., $\log_{10}(P)$) color scheme, and the color bar is capped at $P = 60\%$ or, equivalently at $\log_{10}(60\%) \backsimeq 1.778$ (darkest red), so that the variations of color throughout the North Pacific are clearly visible. Zero probabilities are shown in white, and nonzero probabilities vary from blue to red with increasing values. The same color scheme will be used throughout the remainder of the paper. Figure

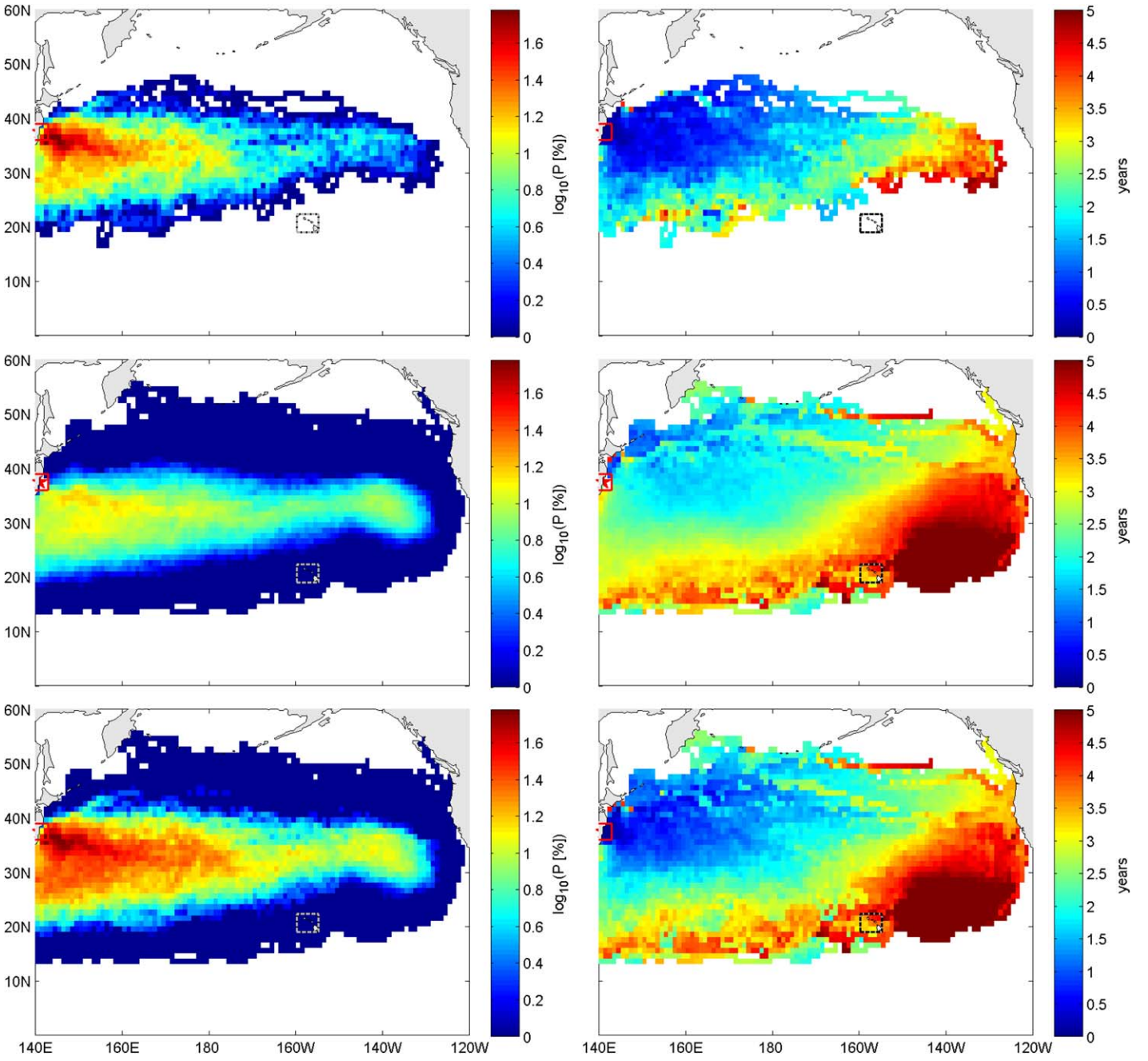

Figure 4. (top) The direct, (middle) one-stop, and (bottom) total probability maps (left) with corresponding travel time maps (right) resulting from application of the two-iteration method to simulated 5 year long trajectories. Each month from October 1992 through September 2007, 25 simulated drifters were released at random locations throughout the North Pacific, for a total of 4500 drifters, and their trajectories were evolved for 5 years using the same velocity field as in Figure 3.

3 suggests that the bulk of trajectories in this calculation move eastward with the Kuroshio Extension, reaching longitudes of approximately 130°W after 5 years, and for the most part stay between 15°N and 45°N throughout this period (see Figure 3, left). However, a smaller number of trajectories enter the Western Subarctic Gyre, reaching latitudes of 60°N. The outline of this recirculation pattern is clearly visible in the northwestern corner of the map (Figure 3).

2.3. Extended Probability Maps: The Two-Iteration Method

The conventional method for computing probabilities, i.e., which was used to produce Figure 3, works well when large numbers of trajectories are available. In reality, however, only about 100 real drifters were ever

released or passed through our source domain near the Fukushima power plant. The probability map computed using equation (2) with these real drifters has only a few nonzero P_{ij}'s and is empty over broad areas of Pacific Ocean. One way to improve the probability map estimation is to modify expression (2) to make use of information about those drifter trajectories that do not necessarily pass through the source domain but instead pass through boxes with nonzero P_{ij}'s. In other words, in addition to the probability P^{direct} (given by equation (2)) that characterizes the percentage of trajectories that go directly from a source box A to a destination box B, one can also compute the probability P^{1stop} to go from A to B indirectly through any other box X. Assuming drifters can get from A to B by either the direct or one-stop route, the total probability P^{tot} can be written as a sum:

$$P^{total} = P^{direct} + P^{1stop}\left(1 - P^{direct}\right). \tag{3}$$

To make further progress, the direct probability can be written as

$$P^{direct}_{A\to B} = \frac{\#\ successful\ \ direct\ \ trajectories}{\#\ direct\ \ trajectories\ \ leaving\ \ A} = \frac{N_{A\to B}}{N_A}, \tag{4}$$

and the indirect probability as

$$P^{1stop}_{A\to B} = \frac{\#\ successful\ \ one\ \ stop\ \ trajectories}{\#\ one\ \ stop\ \ trajectories\ \ leaving\ \ A} = \frac{\sum_X N_{A\to X\to B}}{\sum_X N_{A\to X\to anywhere}} = \frac{\sum_X N_{A\to X} N_{X\to B}}{\sum_X N_{A\to X} N_X}, \tag{5}$$

where $N_{A\to X}$ denotes the number of trajectories going from box A to box X and N_X denotes the number of trajectories leaving box X. The summation in equation (5) is over all boxes X with nonzero $P^{direct}_{A\to B}$. In simple terms, different trajectory segments are stitched together to form longer trajectories and thus obtain a more complete data set. Those trajectories that were used to estimate $P^{direct}_{A\to B}$ are excluded from consideration when computing $N_{X\to B}$ and N_X in equation (4) to avoid possible double counts. The corresponding mean travel time for each bin is estimated as the weighted sum of the direct and one-stop travel times:

$$\overline{T_{A\to B}} = \frac{P^{direct}_{A\to B}\bar{T}^{direct}_{A\to B} + P^{1stop}_{A\to B}\bar{T}^{1stop}_{A\to B} - P^{direct}_{A\to B}P^{1stop}_{A\to B}\left(\bar{T}^{direct}_{A\to B} + \bar{T}^{1stop}_{A\to B}\right)/2}{P^{direct}_{A\to B} + \left(1 - P^{direct}_{A\to B}\right)P^{1stop}_{A\to B}}, \tag{6}$$

where

$$\bar{T}^{direct}_{A\to B} = \frac{\sum T_{successful\ \ direct\ \ trajectories}}{\#\ successful\ \ direct\ \ trajectories} = \frac{\sum T_{A\to B}}{N_{A\to B}} \tag{7}$$

and

$$\bar{T}^{1stop}_{A\to B} = \frac{\sum T_{successful\ \ one\ \ stop\ \ trajectories}}{\#\ successful\ \ one\ \ stop\ \ trajectories} = \frac{\sum_X \left(\sum_{N_{A\to X\to B}} T_{A\to X\to B}\right)}{\sum_X N_{A\to X\to B}} = \frac{\sum_X \left(\sum_{N_{A\to X\to B}} (T_{A\to X} + T_{X\to B})\right)}{\sum_X N_{A\to X\to B}}. \tag{8}$$

Here this method of computing probability and travel time maps through the combination of direct (equations (4) and (7)) and one-stop (equations (5) and (8)) calculations is referred to as the two-iteration method (equations (3) and (6)).

Before applying the two-iteration method to real drifters, we first tested its performance in more idealized settings, where once again 25 simulated drifters were released once per month during 15 years (180 releases in total) from 1992 to 2007 at random locations throughout the North Pacific, totaling 4500 trajectories. As before, each simulated trajectory was integrated for 5 years using the same velocity field used to produce Figure 3. For comparison, we note that this simulated drifter data set is approximately 5 times larger than the real GDP data set. The resulting direct, one-stop and total probability maps along with the corresponding travel time maps are shown in Figure 4. Even in this idealized setting with far more drifter hours of data than are available in reality, the number of trajectories and trajectory segments that are released or pass through the Fukushima source box is limited. Compared to Figure 3, the direct probability and travel time maps in Figure 4 (top) are incomplete and incorrectly predict zero probabilities at many locations throughout the North Pacific. The issue is exacerbated further from the source. The one-stop

Table 1. Pearson Correlation Coefficients Between the Probability Map in Figure 3 and Probability Maps in Figures 4–6

	Direct Map	Two-Iteration
4500 simulated drifters (Figure 4)	0.7	0.88
Simulated GDP drifters (Figure 5)	0.45	0.77
Real GDP drifters (Figure 6)	0.69	0.81

calculation shown in Figure 4 (middle) mitigates the limitations caused by the small number of direct trajectories by successfully filling in missing values, particularly in outlying areas. The resulting total maps (Figure 4, bottom) better resemble the "true" patterns (Figure 3), correctly reproducing all the major features in terms of distribution shape, extent, and color. To quantify the degree of similarity between different probability maps, we have computed Pearson correlation coefficients between different numerical runs. As shown in the top row of Table 1, the correlation coefficient is fairly low (0.7) between the probability map in Figure 3 and the direct probability map in Figure 4 but increases to 0.88 after applying the two-iteration method.

It is evident from Figure 4 that the two-iteration method works well with a large number of long trajectories. In reality, however, even though ~6000 GDP trajectories are available in the North Pacific, many of them are short, that is, the average drifter lifetime is less than a year. To validate the application of the two-iteration method with a limited data set, we performed a more realistic test. Here the distribution of real drifters was mimicked by releasing the simulated drifters at the times and locations of the real drifters. The simulated drifter trajectories were then evolved over the lifespan of the real drifters, thereby producing a simulated version of the GDP drifter data set. Trajectories and trajectory segments prior to 1992 were ignored because velocity fields were unavailable for that time period.

For the simulated GDP data set, only about 60 drifters passed through the Fukushima source area, so the direct probability and travel time maps in Figure 5 (top) are quite deficient, leaving much of the North Pacific blank (i.e., with zero probability). However, with the addition of the one-stop trajectories, the results improve and, even though not quite complete, the details of the total maps shown (Figure 5, bottom) compare much more favorably with Figure 3 than the direct estimates (Figure 5, top). This improvement is quantified in the middle row of Table 1, which shows that the Pearson correlation coefficient between probability maps in Figures 3 and 5 increases from 0.45 for the direct map to 0.77 for the two-iteration probability map.

3. Drifter-Based Estimates of Fukushima-Derived Radionuclide Spread in the Pacific Ocean

With the simulated drifter tests in hand, we proceed by applying the two-iteration method to real GDP drifters. As before, first direct maps are computed (equations (4) and (7)) based on those drifters that pass through the Fukushima source domain (Figure 6, top). These are combined with one-stop results (equations (5) and (8), Figure 6, middle) to obtain total maps (equations (3) and (6), Figure 6, bottom). Similar to the case with simulated drifters (Figure 5), the direct maps in Figure 6 (top) only appear complete close to the Fukushima source domain. Further into the Pacific, the maps develop gaps due to the insufficient number of drifters and their short lifetime. The Pearson correlation coefficient between the direct probability map in Figure 6 (top left) and Figure 3 (left) is 0.69. The GDP one-stop maps (Figure 6, middle) help to fill in these gaps yielding total maps (Figure 6, bottom) with much better spatial coverage and higher Pearson correlation coefficient of 0.81.

Overall, the total real-drifter-based maps in Figure 6 (bottom) agree in shape, extent, and magnitude with the simulated-drifter-based results shown in Figures 3–5. Specifically, the large Pearson correlation coefficient of 0.81 between the probability maps in Figures 5 and 6 (bottom) implies a high degree of similarity between the real and simulated GDP drifters. This similarity suggests that geostrophic and Ekman currents are the two major players governing the motion of the drifters at large scales.

However, comparing the two-iteration real-drifter-based probability map (Figure 6, bottom) to a conventionally computed simulated-drifter-based map (Figure 3) reveals some differences. In particular, the Western Subarctic gyre is much less visible in Figure 6 compared to Figure 3, whereas the Alaskan gyre and the California current systems are more pronounced in Figure 6. Note that similar to Figure 6, the Western Subarctic gyre is also missing in the two-iteration simulated-drifter-based map in Figure 5 suggesting that this is caused by the deficiencies of the drifter data set rather than deficiencies in the velocity field used to

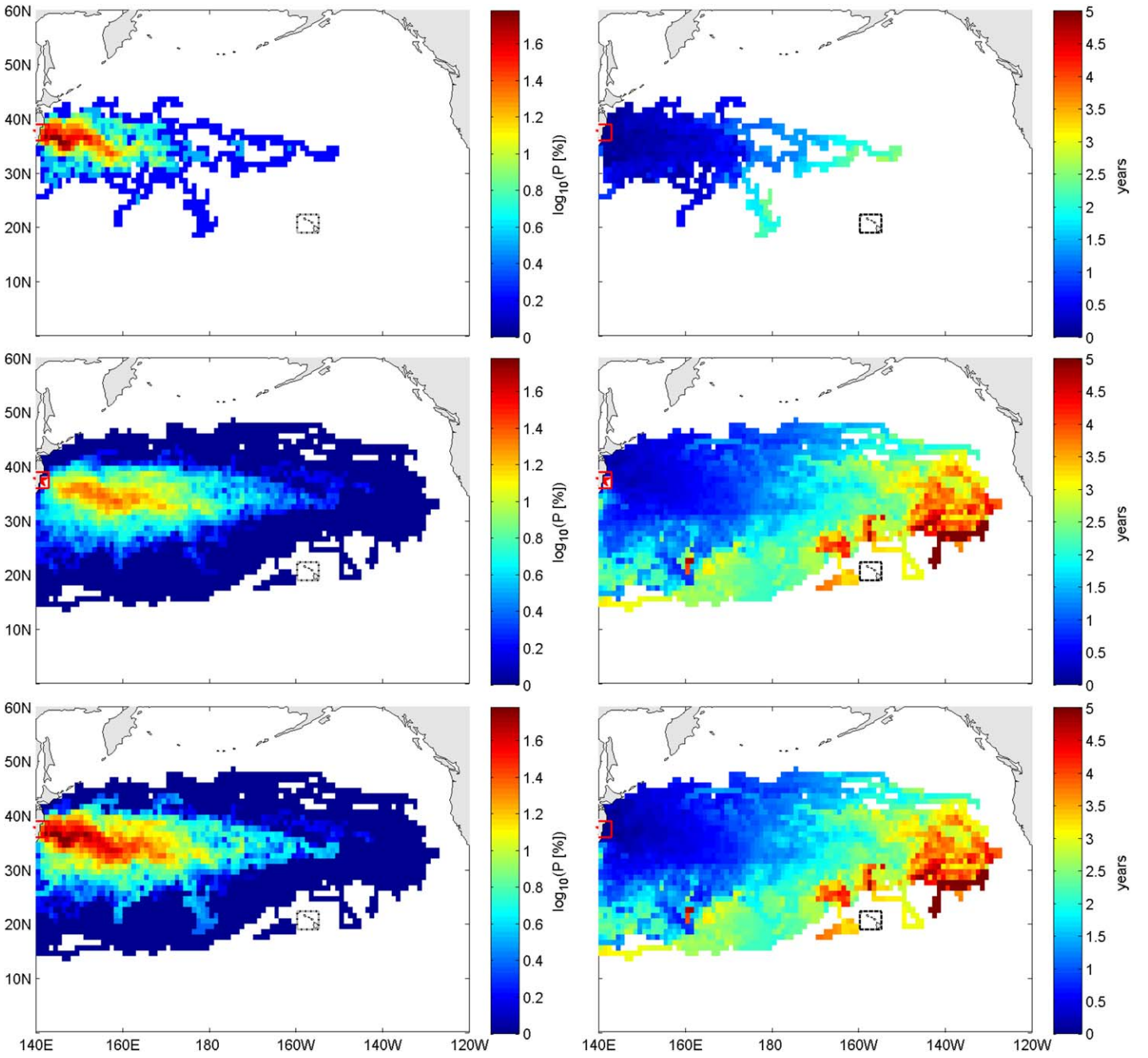

Figure 5. Same as Figure 4 but for the simulated GDP drifter data set, where simulated drifters were released at times and locations matching those of actual GDP drifters, and the simulated trajectories were calculated over the lifespan of the actual drifters.

advect simulated drifters. The somewhat "streakier" appearance of probability maps in Figure 6 compared to the smoother map in Figure 3 is also a direct consequence of the limited number of available real drifter trajectories. Additional analysis (not shown) suggests that agreement with the observed Cs based on the surveys from 2012 and 2013 is worse for the simulated-drifter-based maps than for the real-drifter-based maps, and that unlike the real-drifter-based results that will be described in sections 4 and 5, simulated-drifter-based maps do not reproduce observed arrivals of Fukushima radionuclides off Alaska starting 1.3 years after the accident in June 2013.

Another view of the real-drifter-based results is presented in Figure 7 where the probability map is split into different geographical domains according to the corresponding travel time. In other words, in each subplot

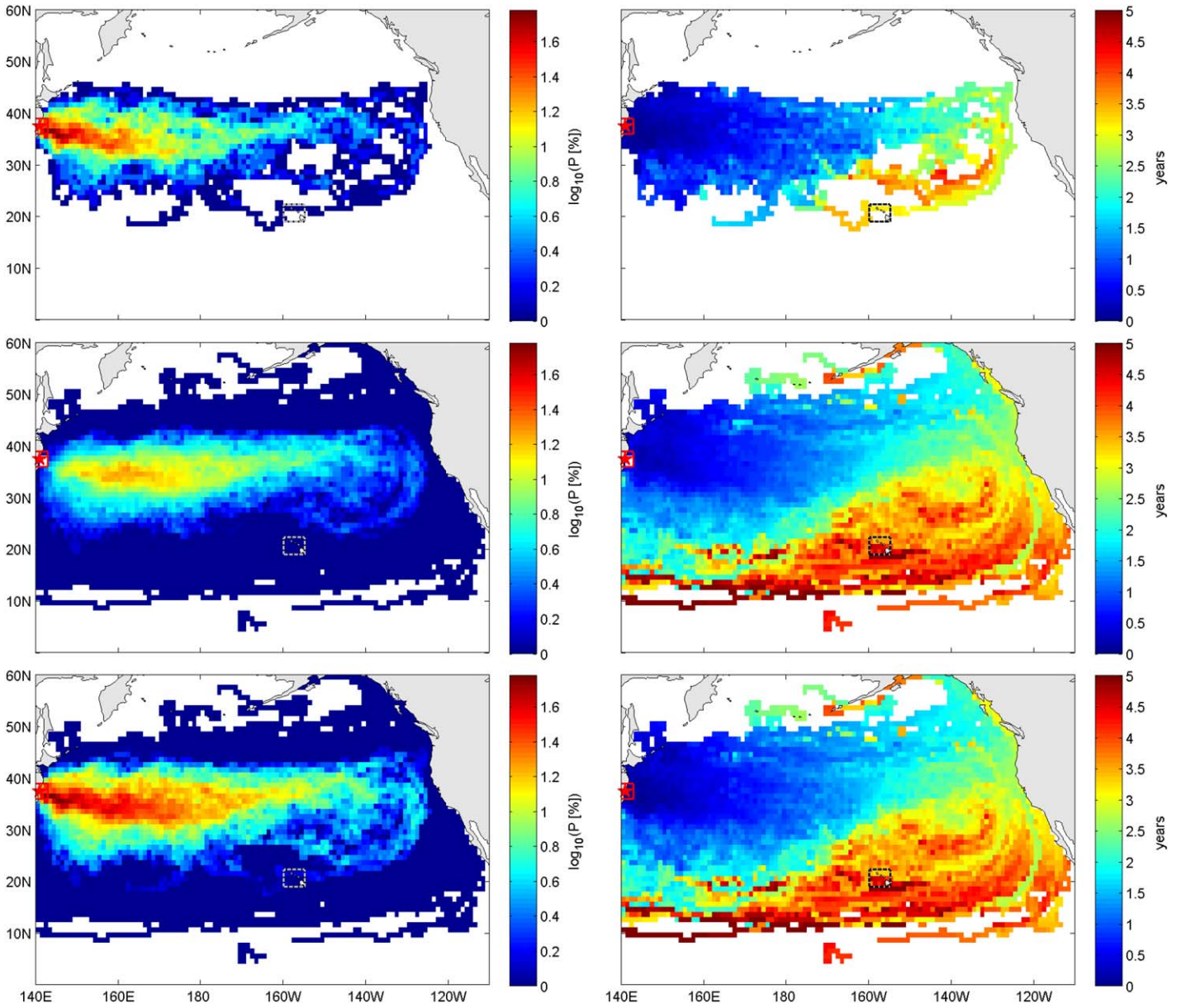

Figure 6. (top) Direct, (middle) one-stop, and (bottom) total probability maps (left) with the corresponding travel time maps (right) resulting from applying the two-iteration method to the GDP drifters.

of Figure 7, we pick only those geographical locations with travel times from T_{min} to T_{max}, thus visualizing the temporal progression of the leading front of the tracer as it spreads out of the Fukushima source area and into different geographical locations throughout the Pacific Ocean. Even with the two-iteration technique, the number of available drifter trajectories is limited, especially for longer travel times. Consequently, with a fixed time interval, as time increases, fewer probability map bins have $T_{min} \leq T \leq T_{max}$, so snapshots of the leading front of the tracer (Figure 7) become increasingly empty (white). To mitigate this issue, we increase the time interval from T_{min} to T_{max} ($T_{min} - T_{max}$) with time so that the statistics of the snapshots do not deteriorate at longer travel times. That is, the integral of the probability is constant across Figure 7.

Initially, the bulk of trajectories move eastward, with some minimal indication of the slight northward spread and entrainment into the Western Subarctic recirculation. The southward spreading of trajectories is initially inhibited by the strong Kuroshio Current and its Extension, which together act as a transport barrier in the western part of the basin. This barrier effect agrees with both observations and model results

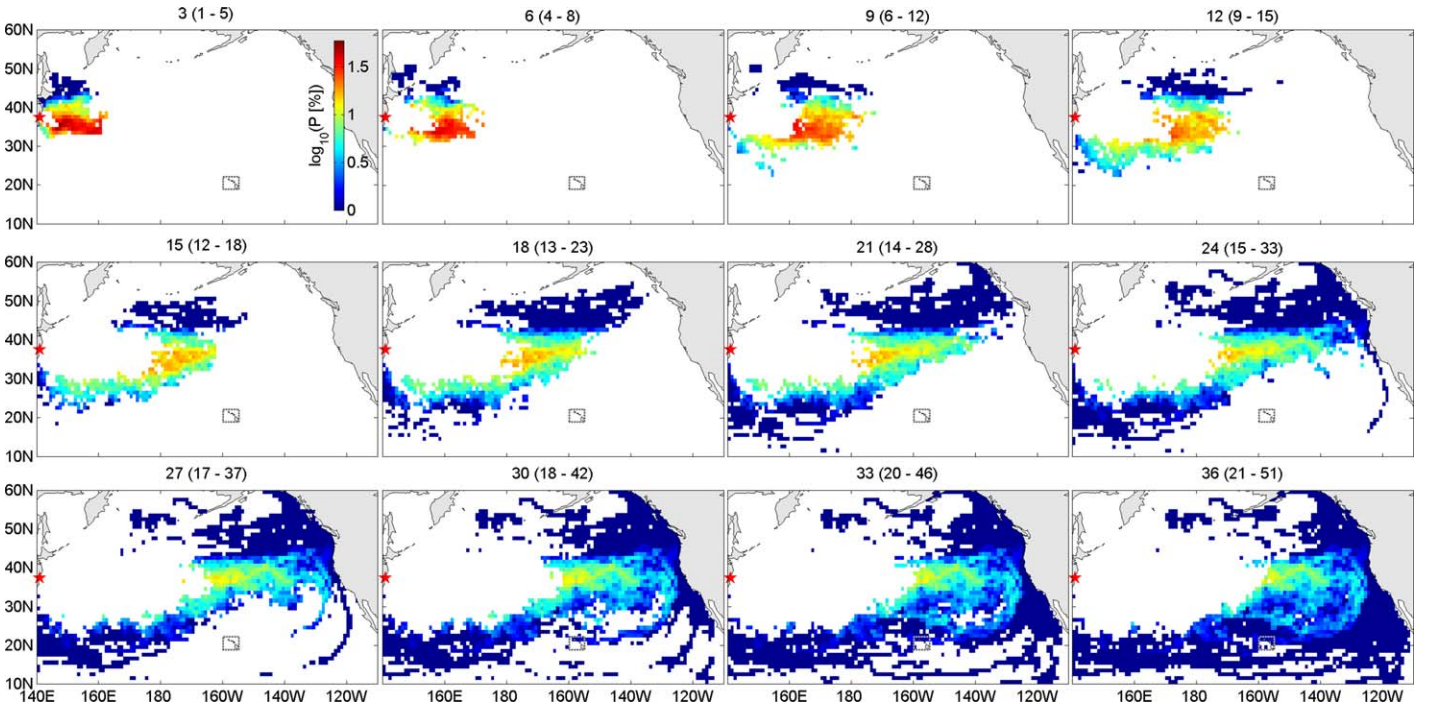

Figure 7. Probability map snapshots (extracted from Figure 6, bottom) showing the progression of a tracer as it spreads out from the Fukushima source area and into the Pacific Ocean with time. Numbers at the top of each figure indicate the average month since start and a delta-time ($T_{min} - T_{max}$) in months, i.e., the first figure is the "snapshot" around month 3 including all drifters with travel times in the time period 1–5 months.

according to *Rypina et al*. [2013], who also reported the mostly eastward spread of contaminated water over the first 3 month after the accident. By 9 months, as the bulk of the distribution travels further east, the Kuroshio Extension slows and becomes more diffuse allowing for more southward cross-jet transport, so nonzero probabilities start to show up south of the Kuroshio Extension. By 18 months, the leading edge of the tracer forms a diagonal front extending from the southwest to northeast. The front continues to move eastward across the Pacific, its northeastern corner following the Alaska Current and starting to curve to make its way into the Alaskan gyre approximately 2 years after the FNPP accident. The peak probability values, however, still remain approximately at the initial latitude (~40°N) at this time. Soon after, at about 27 months, the California Current system starts to advect the tracer into the subtropical gyre. By 3 years, this process is well underway and continues to dominate the distribution for up to 5 years. The time scales longer than 5 years are not well represented by the drifter data set and were not investigated in this study.

4. Comparison With Data

The drifter-based probability maps in Figure 7 (top 4 panels), which can be interpreted as the progression of the leading front of the tracer distribution during roughly the first year after the accident, are in agreement with the observational study by *Aoyama et al*. [2013, their Figures 1–4]. Both our results and Aoyama's consistently indicate that the bulk of the Cs-rich plume traveled eastward between roughly 30°N and 40°N, passing the International Date Line approximately 1 year after the accident.

An opportunity to further validate the drifter-based predictions was created by large-scale North Pacific cruises conducted in 2012 and 2013 [*Kamenik et al*., 2013; S. Yoshida et al., in preparation, 2014]. In 2012, surface water samples were collected by a Sea Dragon cruise (Two Hands Project: www.twohandsproject.org) from Yokohama to Hawaii (June to July 2012) and by a Sea Education Association (SEA: www.sea.edu) cruise from San Diego to Hawaii (October to November 2012). The transect along 30°N in 2013 was conducted as the repeat hydrography line P02 in the North Pacific as part of the U.S. Climate Variability and Predictability (CLIVAR)/Global Ocean Ship-based Hydrographic Investigations (GO-SHIP) programs (March to May 2013). The resulting maps of near-surface ^{134}Cs concentrations are shown in Figure 8 (top). One of the

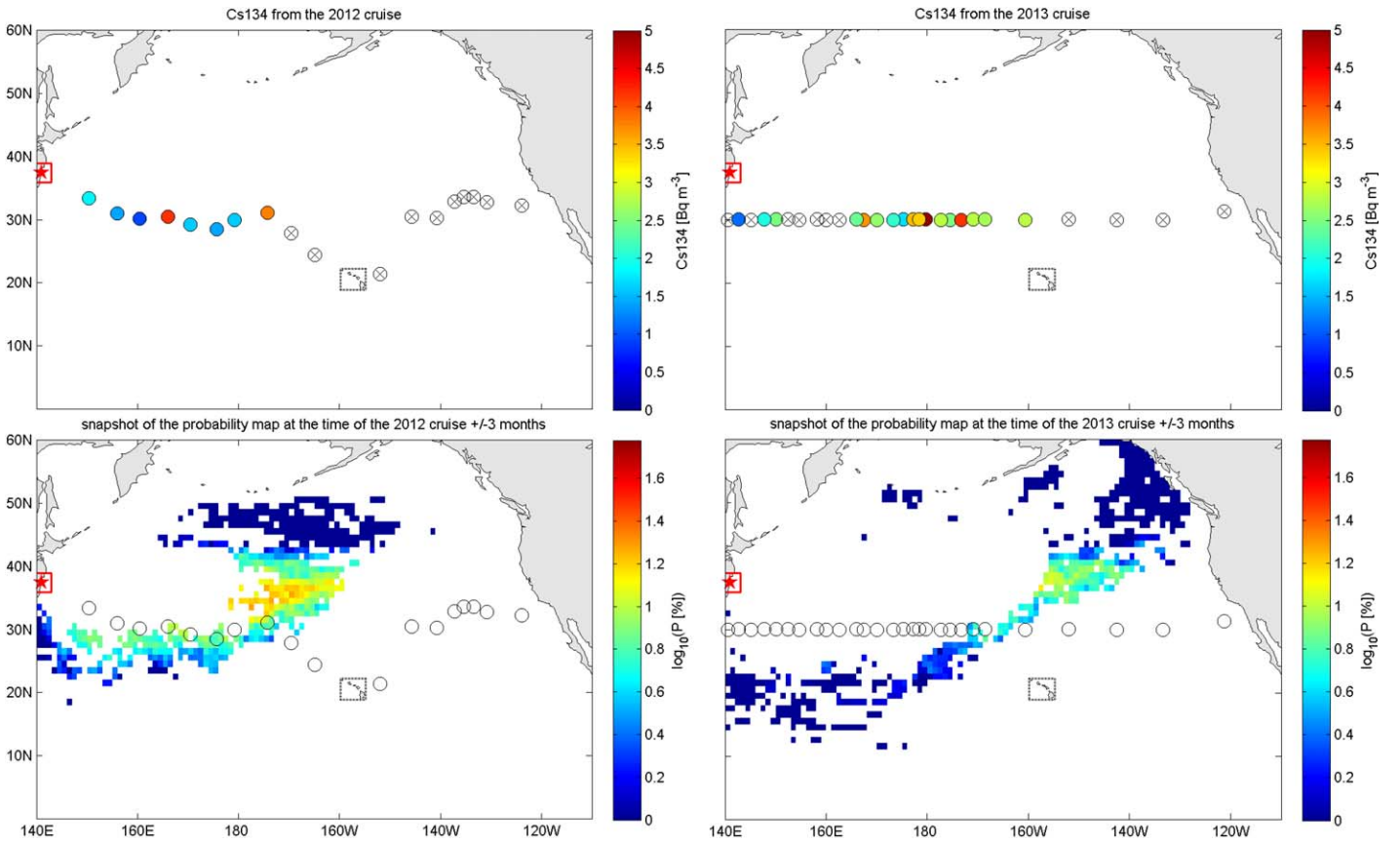

Figure 8. (top) Concentration of ^{134}Cs in the surface waters from the (left) 2012 (Two Hands Project and SEA) and (right) 2013 (CLIVAR P02) cruises and (bottom) a probability map snapshot at the time of each cruise. The circles in the top figures indicate observed ^{134}Cs, while in the bottom figures they indicate station location. We remind the reader that the bottom figures like all previous probability maps indicate probabilities and not ^{134}Cs concentration.

most striking features of these maps is an acutely sharp cutoff of the detectable ^{134}Cs at approximately 175°W in 2012 and around 160°W in 2013, providing an estimate of the temporal progression of the leading edge of the Cs distribution from the Japan coast. A quick visual comparison suggests that the timing of this progression agrees with the general trend seen in the drifter-based maps (Figure 7).

To better quantify the comparison between the observed ^{134}Cs and the drifter-based results, we have constructed probability map snapshots at the times corresponding to the 2012 and 2013 cruises, and superimposed the ship track on color-coded probability maps (Figure 8, bottom). A $\pm$3 month temporal window is used to correspond roughly to the duration of each cruise, and at the same time to allow for reasonable drifter statistics. It can be seen that the last station with detectable ^{134}Cs levels falls directly on top of the leading edge of the cesium front estimated by the drifter-based probability maps at the time of each cruise. Our drifter-based maps also suggest that during both the 2012 and 2013 cruises, the peak in the leading edge of the ^{134}Cs distribution was slightly north of the actual ship track following the northern edge of the Kuroshio Extension across the basin.

Although not visible in the available observations (Figure 8, top) due to the scarcity of observed positions, spreading of radionuclides into the Alaskan Gyre system is indicated by the drifter-based maps in Figure 8 (bottom right) (as well as in Figures 6 and 7). There is a northward spread centered 140°W in agreement with the circulation according to hydrography [*Reid*, 1997] as well as an indication of the coastal current effect. The predicted early arrival of Fukushima radionuclides into the Gulf of Alaska starting 1–1.5 years after the accident is also consistent with the measurements made by the Bedford Institute off Alaska at Station Papa located at 50°N and 145°W, where elevated concentrations of ^{134}Cs at levels exceeding the fallout values were first detected in June 2012 [*Smith and Brown*, 2014; J. N. Smith, Bedford Institute of Oceanography, Canada, personal communication, 2014].

It is important to note that our probability maps assume that the bulk of the radionuclide discharge from the Fukushima power plant occurred by mid-April 2011. In reality, however, the FNPP pipe leakage and ground water discharge continued far beyond this time at more than 10,000 times lower rate than the initial contamination event [*Kanda*, 2013]. The absence of this prolonged leakage in the calculations presented here is likely responsible for zero probabilities close to Fukushima in 2012 and 2013 in our drifter-based maps. In reality, ^{134}Cs was detected at many of the near-shore stations well after the initial event.

5. Summary and Discussion

The goal of this study was to make use of available near-surface drifter trajectories that have been accumulated over decades of fieldwork to shed light on the spreading of the Fukushima-related radionuclides from the Japan coast into the greater Pacific Ocean. Our approach was to approximate the dispersal of a tracer by the spreading of a large number of drifters released near Fukushima and to construct probability maps quantifying where these drifters are expected to be found at some time after their release. This approach has several limitations, a major one being that real drifters are constrained to stay at the ocean surface while the tracer is not and thus may subduct and penetrate into deeper waters with time as suggested by the numerical simulation of *Behrens et al*. [2012] and *Rossi et al*. [2013]. For this reason, our probability maps can only be interpreted as indicators of the near-surface signature of Fukushima-related cesium distribution. The conversion from probability maps to cesium concentration is possible but challenging as it requires knowledge of both the magnitude of the cesium sources as well as the vertical distribution of the tracer in the water column over the full North Pacific. Because the latter is unknown, we did not attempt to perform such a conversion as part of this investigation.

In an idealized case of a large drifter data set with long trajectories, probability maps can be constructed based only on those drifters that are released in or pass by close to the Fukushima source domain. In reality, however, only a small number of such drifters (about 60) are available, and their trajectories average less than 1 year. Thus, the resulting probability maps are deficient and incomplete, with large gaps at many locations particularly further from the Fukushima source domain.

To mitigate this deficiency and improve the probability maps, we made use of the novel two-iteration method that allowed appending the "direct" probability map with the "one-stop" map based on those drifters that pass through geographical locations with nonzero direct probabilities. In other words, we combined segments of trajectories to form more possible paths connecting the source area to different geographical locations throughout the Pacific Ocean. Here we tested this technique both in idealized and more realistic settings in a series of numerical experiments with simulated drifter releases, and concluded that the two-iteration method greatly improves the results.

We have applied the two-iteration method to real drifters from the GDP data set to produce the probability maps predicting the movement of Fukushima-related radionuclides in the ocean over 5 years. We remind the reader that our maps quantify the probability to *initially reach* different geographical areas, and thus illustrate the progression of the *leading edge* of the tracer distribution, rather than show the tracer distribution itself. Sensitivity tests presented in Appendix A show that our maps are not particularly sensitive to changes in the bin size and source domain size.

Overall, our results indicate that during the first few months after the accident, the tracer progresses eastward from the Japan coast, staying north of the Kuroshio Current. Of interest is the sharp cutoff in the distribution to the south, where red colors transition directly into white, as opposed to the more gradual color changes (red to blue to white) observed in the northern part of the tracer distribution over the first 6 months. This sharp cutoff indicates the presence of the strong transport barrier near the Kuroshio Current system over the western North Pacific suggested by earlier observational and model-based studies [*Rypina et al*., 2013]. As the tracer progresses further east, the Kuroshio slows and the barrier weakens, so by 9 months southward spread of the tracer starts to occur. Consistent with *Aoyama et al*. [2013], our drifter-based maps indicate that the Cs-rich waters reach the International Date Line (some 3400 km from the FNPP) between 30°N and 40°N approximately 1 year after the accident. After 1.5 years, the leading edge of the tracer distribution extends diagonally from southwest to northeast. This front moves eastward across the basin, and by 2 years its northeastern part follows the Alaska Current into the Alaskan Gyre. The timing of this predicted early arrival into the northeastern North Pacific is in agreement with available

measurements off Alaska, where Fukushima ^{134}Cs was first detected 1.3 years after the accident in June 2013 [*Smith and Brown*, 2014; Smith, personal communication]. In the south, starting at about 2.5 years and onward, the tracer is advected by the California Current and begins to recirculate counterclockwise in the subtropical gyre, forming the characteristic semicircular shape also found by *Behrens et al*. [2012]. All the described characteristic spatial patterns—the transport barrier associated with the Kuroshio Current, the broadly eastward initial progression of the tracer, and the later splitting of the tracer to the north and south, with the consequent entrainment of the northern part into the Alaskan Gyre and the southern part into the subtropical gyre—are in agreement with the numerical-model-based investigation of the Fukushima-derived tracer dispersal by *Behrens et al*. [2012] and *Rossi et al*. [2013].

Our estimate for the timing of the progression of contaminated waters throughout the North Pacific is fairly similar to that of *Rossi et al*. [2013] and slightly shorter than that of *Behrens et al*. [2012]. These three studies predict that waters containing Fukushima-related radionuclides will cross the basin and reach coastal areas of the west American coast at time scales from 2–3 to 5–6 years depending on latitude, with estimates of *Behrens et al*. [2012] being on the upper side (3–6 years) and our estimates (2–4 years) and those of *Rossi et al*. [2013] (3–5 years) on the lower side. The leading front of the Cs-rich waters is predicted to first reach the northeastern Pacific basin after approximately 2 years, after which the Cs-rich waters enter the Gulf of Alaska and then reach Aleutians. The timing of arrivals to the west coast of North America increases from north to south and varies from about 2–2.5 years at around 50°N to 2.5–3 years at 40°N with later arrivals ($\geq$3.5 years) south of 35°N. Arrivals to Hawaii are predicted after approximately 2.5–4.5 years, which is slightly shorter that 3–5 years predicted by *Behrens et al*. [2012] and *Rossi et al*. [2013].

To summarize, our drifter-based predictions agree well with the model-based results of *Behrens et al*. [2012] and *Rossi et al*. [2013] in terms of patterns but suggest a somewhat faster time scales for the propagation of the contaminated waters across the North Pacific. It is important to note that due to the limited number of available drifter trajectories, our probability and travel time maps are best suited for interpreting the overall large-scale patterns rather than looking at individual arrivals at some exact locations. Coastal areas, where the number of available drifters is particularly limited and where the three-dimensional effects of up-/downwelling cannot be ignored are not well represented in our maps.

The drifter-based predictions of the progression of the contaminated waters across the basin with time were shown to compare favorably with the available 2012 and 2013 measurements of near-surface Fukushima-related ^{134}Cs. Both the ^{134}Cs measurements and our drifter-based estimates indicate that over the course of 1 year the leading edge of the ^{134}Cs distribution travels eastward approximately 1500 km from about 175°W longitude in 2012 to about 160°W in 2013. The positive agreement between the measured and predicted leading edge of the ^{134}Cs distribution (Figure 8) is reassuring and suggests that drifter data sets could be a useful point of validation for model-based studies and an important source of information about the future progression of the Fukushima-related radionuclides in their own right.

Contaminated waters are expected to subduct as they move offshore, especially as they pass through the mode formation region with deep mixed layers and outcropping isopycnals to the east of FNPP. This vertical penetration, which is absent in our drifter-based analysis, could affect both the near-surface tracer concentrations and the timing of tracer's progression through the Pacific Ocean. Note however, that because oceanic currents generally moderate with depth, the leading edge of the tracer distribution (which is the focus of our analysis) is still likely to be found near the surface, even though the tracer concentration might be higher at depth. This is especially true for the eastern leading edge carried out by Kuroshio Extension, whereas the timing of the southward progression is less clear. It has been shown that near the surface the Kuroshio and its extension act as transport barriers, and subduction could provide a potentially faster route across Kuroshio at depth. Note also that because isopycnals lying below 200 m in the west do not outcrop in the middle of the North Pacific [*Talley*, 2007] until they reach the eastern side of the basin, and because waters subducted below that depth in the west are expected, to a first approximation, to follow the isopycnals, they are not expected to re-enter the near-surface mixed layer midbasin. Upwelling in the eastern part of the North Pacific basin near the Californian coast could potentially bring the subducted cesium plume back to the ocean surface [*Rossi et al*., 2013]. However, this route would again be slower than the surface route and thus is not expected to affect the leading edge of the cesium distribution. Therefore, ignoring the vertical penetration of radionuclides is not expected to strongly influence our results. Positive agreement between our results and the observed progression of Fukushima-related cesium support the above arguments.

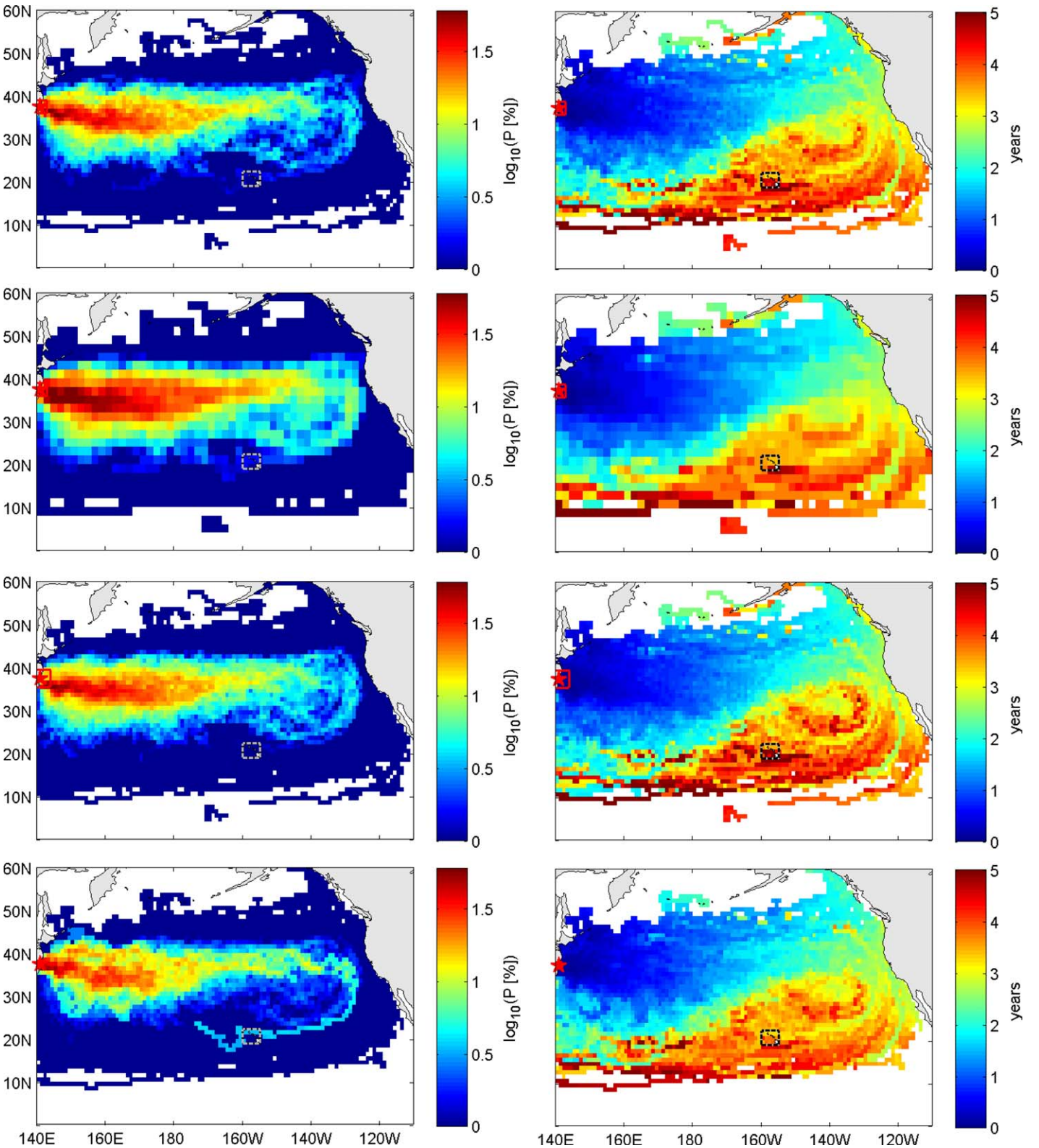

Figure A1. (left) Two-iteration probability maps and (right) the corresponding travel time maps for various bin sizes and source domain sizes. Row 1: standard run (same as Figure 6, bottom) with 1° × 1° bins and 2° × 3° source domain. Row 2: low resolution run with 2° × 2° bins. Row 3: large 3° × 4° source domain run. Row 4: small 1° × 1.5° source domain run.

In our analysis, we employ a statistical approach where we simultaneously use all available drifters independently of their release timing, thus averaging over different seasons and years. Additional analysis (not shown) where we recalculated Figure 3 using trajectory releases during the three spring months only (March/April/May) instead of year-round releases suggest that seasonal changes have only minimal effect on our maps. We anticipate that seasonal effects might have a stronger influence on the three-dimensional cesium distributions rather than on the surface signature of the leading edge of the cesium plume.

The two-iteration method could be easily generalized to multiple iterations by looking at indirect trajectory paths with more than one intermediate stop. In other words, more than two trajectory segments could be stitched together to obtain all possible drifter paths connecting bins A and B. However, drifters used to produce prior iterations should be excluded from all subsequent iterations to avoid double counts of trajectories, and therefore fewer and fewer data points remain for the higher-order iterations. For this reason, the higher-order iterations are only practical when extensive data sets are available. In the case of the GDP data set, the second iteration utilizes the majority of available drifter trajectories, so a third iteration does not lead to further improvements in the probability maps.

Appendix A: Sensitivity Analysis

Sensitivity of the probability maps to the bin size and the size of the source domain has been investigated in Figure A1 by recalculating the probability maps using larger $2^\circ \times 2^\circ$ bins instead of the $1^\circ \times 1^\circ$ bins used in the standard run (Figure 6), and using both larger and smaller source domains (3° longitude $\times$ 4° latitude and 1° longitude $\times$ 1.5° latitude, respectively) instead of 2° longitude $\times$ 3° latitude as in the standard run. The Pearson correlation coefficient between the probability maps resulting from the standard and large bin size runs (the first and second rows of Figure A1) is 0.94, suggesting that doubling the bin size in both latitude and longitude does not lead to any major qualitative changes in the resulting probability map. This result implies that trajectory statistics are satisfactory in our standard run. Similarly, the probability map is fairly insensitive to the variations of the source domain size within reasonable limits, as the correlation coefficients between the standard and the large/small source domain runs are 0.97 and 0.92, respectively. Note, however, that drifter statistics gets poorer for the small source domain run as only 37 trajectories pass through the source box in the latter case, compared to 128 for the standard run, and 246 for the large source domain.

Acknowledgments

This work was supported by the grant OCE-1356630 from the National Science Foundation. Data for cesium isotopes was supported by grants from the Gordon and Betty Moore Foundation (grant GBMF3007) and the Deerbrook Charitable Trust. We also thank the Two Hands Project and the Sea Education Association for additional sampling collections, and John Smith (Bedford Institute of Oceanography, Canada) for sharing the information about the observational evidence for the early arrival of Fukushima radionuclides into the Alaskan Gyre. The cesium data used to produce Figure 8 are available at http://www.ourradioactiveocean.org/results.html; the geostrophic velocity estimates are available from the AVISO website http://aviso.altimetry.fr/index.php?id=1271; the wind stress data are available from the NOAA NCEP/NCAR website http://www.esrl.noaa.gov/psd/data/gridded/data.ncep.reanalysis.derived.surface-flux.html.

References

Aoyama, M., D. Tsumune, and Y. Hamajima (2012), Distribution of ^{137}Cs and ^{134}Cs in the North Pacific Ocean: Impacts of the TEPCO Fukushima-Daiichi NPP accident, *J. Radioanal. Nucl. Chem.*, *296*, 535–539, doi:10.1007/s10967-012-2033-2.

Aoyama, M., M. Uematsu, D. Tsumune, and Y. Hamajima (2013), Surface pathway of radioactive plume of TEPCO Fukushima NPP1 released 134Cs and 137Cs, *Biogeosciences*, *10*, 3067–3078, doi:10.5194/bg-10-3067-2013.

Behrens, E., F. U. Schwarzkopf, J. F. Lübbecke, and C. W. Böning (2012), Model simulations on the long-term dispersal of ^{137}Cs released into the Pacific Ocean off Fukushima, *Environ. Res. Lett.*, *7*, 1–10.

Buesseler, K., M. Aoyama, and M. Fukasawa (2011), Impacts of the Fukushima nuclear power plants on marine radioactivity, *Environ. Sci. Technol.*, *45*, 9931–9935.

Dietze, H., and I. Kriest (2012), ^{137}Cs off Fukushima Dai-ichi, Japan—Model based estimates of dilution and fate, *Ocean Sci.*, *8*, 319–332.

Estournel, C., et al. (2012), Assessment of the amount of cesium-137 released into the Pacific Ocean after the Fukushima accident and analysis of its dispersion in Japanese coastal waters, *J. Geophys. Res.*, *117*, C11014, doi:10.1029/2012JC007933.

Honda, M. C., T. Aono, M. Aoyama, Y. Hamajima, H. Kawakami, M. Kitamura, Y. Masumoto, Y. Miyazawa, M. Takigawa, and T. Saino (2012), Dispersion of artificial caesium-134 and −137 in the western North Pacific one month after the Fukushima accident, *Geochem. J.*, *46*, e1–e9.

Jayne, S. R., et al. (2009), The Kuroshio Extension and its recirculation gyres, *Deep Sea Res., Part I*, *56*, 2088–2099.

Kamenik, J., H. Dulaiova, K. O. Buesseler, S. M. Pike, and K. Stastna (2013), Cesium-134 and 137 activities in the central North Pacific Ocean after the Fukushima Dai-ichi nuclear power plant accident, *Biogeosciences*, *10*, 6045–6052.

Kanda, J. (2013), Continuing ^{137}Cs release to the sea from the Fukushima Dai-ichi Nuclear Power Plant through 2012, *Biogeosci. Discuss.*, *10*, 3577–3595, doi:10.5194/bgd-10-3577-2013.

Kawamura, H., T. Kobayashi, A. Furuno, T. In, Y. Ishikawa, T. Nakayama, S. Shima, and T. Awaji (2011), Preliminary numerical experiments on oceanic dispersion of ^{131}I and ^{137}Cs discharged into the ocean because of Fukushima Daiichi nuclear power plant disaster, *J. Nucl. Sci. Technol.*, *48*, 1349–1356.

Macdonald, A. M., S. Mecking, P. E. Robbins, J. M. Toole, G. C. Johnson, L. Talley, M. Cook, and S. E. Wijffels (2009), The WOCE-era 3-D Pacific Ocean circulation and heat budget, *Prog. Oceanogr.*, *82*, 281–325.

Masumoto, Y., et al. (2012), Fukushima Daiichi: Oceanic dispersion simulations of 137Cs released from the Fukushima Daiichi nuclear power plant, *Elements*, *8*, 207–212.

Nakano, M., and P. P. Povinec (2012), Long-term simulations of the 137Cs dispersion from the Fukushima accident in the world ocean, *J. Environ. Radioact.*, *111*, 109–115, doi:10.1016/j.jenvrad.2011.12.001.

Qiu, B. (2001), Kuroshio and Oyashio Currents, in *Encyclopedia of Ocean Sciences*, edited by J. H. Steele, pp. 1413–1425, Academic Press, doi: 10.1006/rwos.2001.0350.

Qiu, B., and S. Chen (2005), Variability of the Kuroshio Extension jest, recirculation gyre and mesoscale eddies on decadal timescales, *J. Phys. Oceanogr.*, *35*, 2090–2103.

Ralph, E. A., and P. P. Niiler (1999), Wind-driven currents in the tropical Pacific, *J. Phys. Oceanogr.*, *29*, 2121–2129.

Reid, J. L. (1997), On the total geostrophic circulation of the Pacific Ocean. Flow patterns, *tracers and transports. Prog. Oceanogr.*, *39*, 263–352.

Rossi, V. E., V. Sebille, A. S. Gupta, V. Garon, and M. England (2013), Multi-decadal projections of surface and interior pathways of the Fukushima Cesium-137 radioactive plume, *Deep Sea Res., Part I*, *80*, 37–46.

Rypina, I. I., L. J. Pratt, and M. S. Lozier (2011), Near-surface transport pathways in the North Atlantic ocean, *J. Phys. Oceanogr.*, *41*, 911–925.

Rypina, I. I., S. R. Jayne, S. Yoshida, A. M. Macdonald, E. Douglass, and K. Buesseler (2013), Short-term dispersal of Fukushima-derived radionuclides off Japan: Modeling efforts and model-data intercomparison, *Biogeosciences*, *10*, 1517–1550.

Smith, J. N., and R. M. Brown (2014), Time series measurements of the arrival of Fukushima 137Cs on line P in the eastern North Pacific Ocean, paper presented at 2014 Ocean Sciences Meeting, ASLO, TOS and AGU, Hawaii Convention Center, Honolulu, Hawaii, USA.

Stohl, A., P. Seibert, G. Wotawa, D. Arnold, J. F. Burkhart, S. Eckhardt, C. Tapia, A. Vargas, and T. J. Yasunari (2012), Xenon-133 and caesium-137 releases into the atmosphere from the Fukushima Dai-ichi nuclear power plant: Determination of the source term, atmospheric dispersion, and deposition. *Atmos. Chem. Phys.*, *12*, 2313–2343. doi:10.5194/acp-12-2313-2012.

Talley, L. D. (2003), Shallow, intermediate and deep overturning components of the global heat budget, *J. Phys. Oceanogr.*, *33*, 530–560.

Talley, L. D. (2007), *Hydrographic Atlas of the World Ocean Circulation Experiment (WOCE). Volume 2: Pacific Ocean*, edited by M. Sparrow, P. Chapman, and J. Gould, Int. WOCE Proj. Off., Southampton, U. K.

Talley, L. D., Y. Nagata, M. Fujimura, T. Iwao, T. Kono, D. Inagake, M. Hirai, and K. Okuda (1995), North Pacific intermediate water in the Kuroshio/Oyashio mixed water region, *J. Phys. Oceanogr.*, *25*, 475–501.

Talley, L. D., G. L. Pickard, W. J. Emery, and J. H. Swift (2011), *Descriptive Physical Oceanography: An Introduction*, 6th ed., 555 pp., Elsevier, London, U. K.

Tomosada, A. (1986), Generation and decay of Kuroshio warm-core rings, *Deep Sea Res., Part A*, *33*, 1475–1486.

Tsumune, D., T. Tsubono, M. Aoyama, and K. Hirose (2012), Distribution of oceanic ^{137}Cs from the Fukushima Dai-ichi Nuclear Power Plant simulated numerically by a regional ocean model, *J. Environ. Radioact.*, *111*, 100–108.

Tsumune, D., T. Tsubono, M. Aoyama, M. Uematsu, K. Musumi, Y. Maeda, Y. Yoshida, and H. Hayami (2013), One-year, regional-scale simulation of 137Cs radioactivity in the ocean following the Fukushima Dai-ichi Nuclear Power Plant accident, *Biogeosciences*, *10*, 5601–5617.

Wijffels, S. E., M. M. Hall, T. Joyce, D. J. Torres, P. Hacker, and E. Firing (1998), Multiple deep gyres of the western North Pacific: A WOCE section along 149°E, *J. Geophys. Res.*, *103*, 12985–13009.

Whalen, C. B., L. D. Talley, and J. A. MacKinnon (2012), Spatial and temporal variability of global ocean mixing inferred from Argo profiles, *Geophys. Res. Lett.*, *39*, L18612, doi:10.1029/2012GL053196.